Nano-Optical Tweezing of Single Proteins in Plasmonic Nanopores

Verschueren, Daniel; Shi, Xin; Dekker, Cees

Important note
To cite this publication, please use the final published version (if applicable).
Please check the document version above.

Nano-Optical Tweezing of Single Proteins in Plasmonic Nanopores

Daniel Verschueren, Xin Shi, and Cees Dekker*

Single-molecule sensing technologies aim to detect and characterize single biomolecules, but generally need labeling while the measurement times and throughput are severely restricted by a lack of positional control over the molecule. Here, a plasmonic nanopore biosensor is reported where single molecules can be electrophoretically delivered into a nanopore sensor with a plasmonic nanoantenna that is used to optically trap single molecules for extended measurement times. Using the light transmission through the antenna as read-out, optical trapping of 20 nm diameter polystyrene nanoparticles and individual beta-amylase proteins, a 200 kDa enzyme, in the plasmonic nanoantenna are demonstrated. Application of an electrical bias voltage allows the increase of the event rate over an order of magnitude as well as shorten the residence time of the proteins in the plasmonic nanopore as they can controllably be drawn out of the trap by electrical forces. Trapping is found to be assisted by protein–surface interactions and trapped proteins can denature on the nanopore surface. The integration of two single-molecule sensors, a plasmonic nanoantenna and solid-state nanopore, creates independent control handles at the single-molecule level—the optical trapping force and electrophoretic force—which provides augmented control over single molecules.

1. Introduction

Universal label-free detection and characterization of single biomolecules, in particular proteins, is a grand ambition in the development of diagnostic sensors.[1] Beyond the obvious advantage that single-molecule biosensors feature ultimate sensitivity with detection at the fundamental limit of one single molecule, such sensors would be able to spot rare aberrant biomolecules in an abundant background of healthy ones,[2] probe substructure of single molecules,[3] and allow to study behavior of single-molecular interactions,[4] ideally all without the need for chemical labeling. Two important approaches that are being explored to achieve such sensors are plasmonic nanoantenna apertures[4] and nanopores, both biological[5] and solid-state nanopores.[6] The core of all these single-molecule sensors

is a nanoscale detection volume that approaches the size of the biomolecule to be probed, thus enhancing the measurement signal and reducing background from other components in the solution.[7] Despite their impressive achievements, both sensor types also face limitations, mostly due to a lack of full motion control of the biomolecule that results in diffusion-controlled sensor response times,[8] low temporal resolution,[9] and inadequate sensor specificity.[10]

More specifically, biological and solid-state nanopores are nanoscale openings in a thin membrane that electrophoretically transport biomolecules toward the sensing region via an externally applied bias voltage. This active transport results in great sensor response times and has been used in the past decade to characterize protein,[11,12] DNA,[13] and protein–DNA interactions.[14,15] However, the mode of transport unavoidably leads to an uncontrollably fast passage of the molecules through the sensing region and high translocation speeds that lead to a limited temporal resolution in the ionic-current readout.[9] Some strategies to reduce this fast speed have been employed,[16,17] but these require labeling and failed to demonstrate full external motion control.

Alternatively, plasmonic nanotweezers have demonstrated the capacity to retain small particles and biomolecules in their sensing volume indefinitely[18–21] through optical trapping.[22] These gold nanoantenna sensors operate via localized surface-plasmon resonances that are light-driven coherent electron oscillations at a metal–dielectric interface. Impinging light is used to excite the resonances to concentrate the electromagnetic field into nanoscale volumes, so-called hotspots, thus generating extreme electric field gradients that allow optical trapping[23] to provide ample readout time of single biomolecules. The presence of the biomolecules trapped in the hotspot can be detected through a shift in the plasmon resonance induced by a local change in the refractive index (RI) in the hotspot of the antenna.[10] The optical transmission (OT) through the subdiffraction-limit-sized nanoaperture communicates this resonance shift to the far field, whereby the biomolecule can be monitored.[24] This approach has been used to reveal protein dynamics[25] and interactions,[26] but the sensor design condemns the user to inextricably long wait times[27] as it relies on the spontaneous diffusion of molecules into the hotspot, and furthermore does not allow for the perturbation of the molecule under study.

Dr. D. Verschueren, Dr. X. Shi, Prof. C. Dekker
Department of Bionanoscience
Kavli Institute of Nanoscience
Delft University of Technology
Van der Maasweg 9, 2629 HZ, Delft, The Netherlands
E-mail: c.dekker@tudelft.nl

The ORCID identification number(s) for the author(s) of this article can be found under https://doi.org/10.1002/smtd.201800465.

Here, we combine both approaches and propose a plasmonic nanopore sensor, an integration of a plasmonic nanoaperture and a nanopore, to overcome the limitations that each sensor bears separately and create a new method for single-molecule manipulation. The electrophoretic force from the nanopore and the optical trapping force from the nanoaperture constitute two independent control handles at the single-molecule level that, respectively, can pull molecules toward the sensor and retain them there. Ultimately, the proposed single-molecule manipulator enables to grab single molecules from solution, and then trap them in the sensor to observe their structural characteristics and native dynamics, and finally expel them after investigation. This creates opportunities for the characterization of protein solutions for diagnostics,[11] the study of protein–ligand interactions for drug screening,[4] and a system for biophysical investigation of protein folding,[28] all without any need for labeling.

Our plasmonic nanopore biosensor is an inverted-bowtie shaped nanoaperture that penetrates both a gold film and the supporting silicon-nitride membrane, creating a plasmonic nanopore that can be excited optically and biased electrically. Using the OT through the nanoaperture as a readout (**Figure 1**A), we first demonstrate the nanotweezing capability of the plasmonic nanopore by trapping 20 nm polystyrene (PS) nanoparticles inside the nanopore with residence times up to seconds. Subsequently, we show that the plasmonic nanopore can be used to detect and trap single beta-amylase proteins, where the polarity of the detected optical signals is correctly predicted from the simulated plasmon resonance peak wavelength of the nanostructure. The optical trapping leads to extended residence times of the protein, while the detailed analysis of the trapping events in the plasmonic nanopore indicates that surface interactions play a significant role in the process. Finally, we characterize the protein detection signal under the application of a transmembrane bias voltage and find that the residence times of the protein decrease, whereas the event rates increase with increasing bias. By using the laser to optically hold biomolecules and the DC bias voltage to alter the protein's residence times and event rates, these plasmonic nanopores thus demonstrate augmented control of the molecules inside the sensor and their motion toward it.

2. Results and Discussion

2.1. Inverted-Bowtie Plasmonic Nanopores for Optical Trapping

The plasmonic nanopore sensor relies on the electrical delivery of molecules or nanoparticles to the nanopore, the excitation of surface plasmons in a gold nanostructure for nano-optical trapping, and on the collection of enhanced OT signal through the inverted-bowtie nanoantenna for readout. Figure 1A shows a schematic description on how this is achieved in practice. A device containing an inverted-bowtie plasmonic nanopore is sandwiched in a liquid-filled flow cell that is mounted in between two objectives. We use a high NA 60× objective to focus the incident 1064 nm wavelength laser light onto a single nanoantenna, and a low NA 10× objective to collect light transmitted through the antenna and focus it onto an avalanche photo diode (APD). Near-field focusing by the antenna of the incident optical field to a nanosized hot-spot permits optical nanotweezing of small nano-objects like single proteins, whereupon changes in the light transmitted through the antenna report on the presence of the object. The advantages that this all-optical readout offers over traditional ionic-current sensing are outlined elsewhere.[29,30] Notably, the plasmonic nanopore chip separates two fluidic reservoirs in a custom-made flow cell, which allows for a variable bias voltage to be applied across the membrane and an electrophoretic force to be acted on the object (see Experimental Section for details).

Figure 1B shows a schematic of the optical nanoantenna, with the definition of various geometrical parameters indicated in the figure. The nanoantenna is an inverted-bowtie shaped aperture in a 100 nm/20 nm thick gold/silicon-nitride film, with typical dimensions of a 60 nm side length, 140 nm width, and 20 nm gap (see Figure 1B). Its ≈20 nm gap is chosen to, at the same time, fit ≤20 nm-in-diameter nano-objects and maximize the plasmon focusing of the optical field. Figure 1C shows a finite-difference time-domain (FDTD) simulation (see Experimental Section) of the amplitude of the optical near field of the antenna excited in longitudinal polarization (as indicated in Figure 1B). This clearly illustrates the field confinement to the gap and shows an electric field enhancement of up to 20 times the incident field strength. For the orthogonal
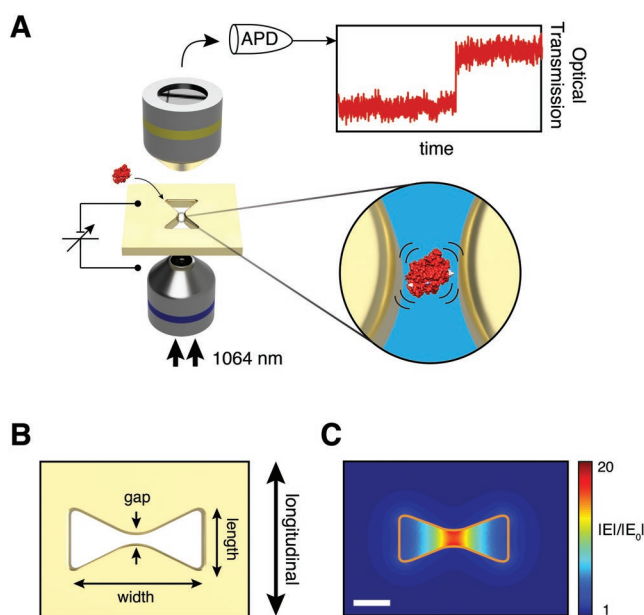

Figure 1. Inverted-bowtie plasmonic nanopore system for optical protein trapping. A) Schematics of the plasmonic nanopore experimental setup, where a protein is optically trapped and monitored in a plasmonic nanopore, possibly manipulated by the application of a variable bias voltage across the pore. B) Schematic of a through-hole inverted-bowtie nanoantenna. The definition of the geometrical design parameters and the polarization direction is indicated in the figure. C) Simulated normalized electric-field distribution of the geometry outlined in orange. Field confinement and enhancement up to 20 times in the gap region is clearly illustrated. Scale bar is 40 nm.

**ADVANCED
SCIENCE NEWS**

www.advancedsciencenews.com

**small
methods**

www.small-methods.com

transverse direction, an enhancement is virtually absent $\left(\frac{E}{E_0} < 0.5 \text{ inside the aperture}\right)$, as seen in simulations reported in Section S1 in the Supporting Information.

Plasmonic nanoantenna arrays are fabricated by first performing electron-beam lithography on a 20 nm thin freestanding SiN membrane and reactive-ion etching to create an array of inverted-bowtie shaped holes within the membrane. Subsequent evaporation of 100 nm gold onto the membrane leads to a SiN/gold film that is perforated with bowtie-shaped apertures (see Experimental Section for fabrication details).

Figure 2A shows a bright field image of a plasmonic nanopore membrane of ≈30 × 30 μm², with two large markers (4 × 4 μm² square apertures) clearly visible, which are used for detector alignment. The plasmonic nanoantennas can be discerned as dots that are arranged in rows on the membrane, where every antenna is spaced at least 3 μm from its neighbor to prevent mutual optical coupling or simultaneous excitation of multiple antennas during experiments. Each row has slightly different design parameters, resulting in slightly reduced scattering for rows that run closer to the large 4 × 4 μm apertures. The zooms show transmission electron microscope (TEM) images of two antennas from this sample, clearly revealing the resulting geometries. Please note a difference in gap size: 15 nm for antenna #1 (top zoom) and 25 nm for antenna #2 (bottom zoom). The typical standard deviation in the

geometrical parameters that are realized within a row (i.e., with the same design parameters) is 7 nm and the sample-to-sample variation of the average values is smaller than this (see additional TEM images in Section S2 in the Supporting Information). Our nanostructures have roughly straight vertical walls resulting from the reactive-ion etching[31] and subsequent gold evaporation. Due to the slight differences in resulting geometries, about 1 in 4 antennas on each sample produce trapping signals (i.e., in total 5 to 10 antennas per membrane).

The TEM images allow us to directly simulate, using an FDTD solver (see Experimental Section), the optical response of any plasmonic nanoantenna with its actual exactly realized dimensions, without the need for geometrical approximations of the average shape. The results of the simulation of the OT spectrum when excited in longitudinal polarization are shown in Figure 2B for the particular antennas #1 and #2 displayed in Figure 2A. Both antennas show a clear resonance peak in the transmission, with an ≈100 nm full-width-at-half-maximum. A clear difference in resonance wavelength can be observed; however, antenna #1 (Figure 2B, left) has a resonance at 1150 nm, i.e., at a longer wavelength than the 1064 nm laser wavelength (indicated with a black solid line), whereas antenna #2 (Figure 2B, right) has a resonance at 950 nm, i.e., to the blue of the laser line. Since the gap for antenna #1 is smaller than for antenna #2, a resonance at a longer wavelength is indeed expected since a smaller gap increases the effective antenna length.[32] Note that the position of the resonance peak with respect to the laser line will determine whether the presence of the analyte, which induces a redshift of the resonance, causes an increase or decrease in the OT:[18] a resonance to the blue of the excitation laser will show transmission increases upon particle insertion in the antenna (i.e., for structure #2), whereas a resonance to the red of the excitation laser will show decreases (i.e., structure #1).
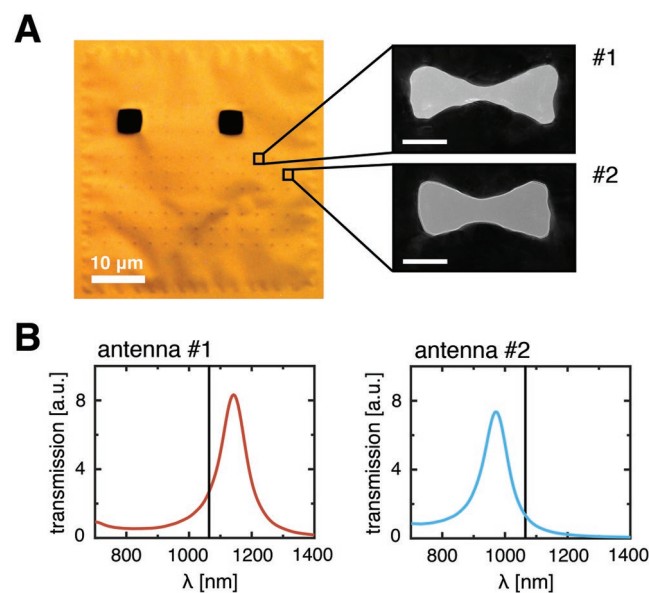
2.2. Nanoplasmonic Trapping of 20 nm Polystyrene Beads

To demonstrate the optical nanotweezing capabilities of our inverted-bowtie nanostructures, we performed nanotweezing experiments on 20 nm PS beads.[21,33,34] **Figure 3** displays OT time traces during a trapping experiment, in the absence of any bias voltage. Figure 3A shows a typical ≈1 s trapping event and a zoom thereof, indicating that PS beads can be optically confined into the plasmonic nanopore. The event is marked by a sudden increase of around 3% in the OT through the nanostructure and is characterized by an increase of the fluctuations in the OT intensity that originate from hopping between two different levels (see zoom in the lower panel of Figure 3A). This can be attributed to the trapping of two PS beads that reside in the nanogap simultaneously, as reported previously,[21] where the presence of one nanoparticle strengthens the optical trap for the other, thus creating a more stable trap for both.[21] Indeed, single-level events are observed, suggestive of the trapping of a single PS bead, but these generally last much shorter than the two-level events. The event sequences that we observe support the dual-trapping hypothesis. For example, the event in Figure 3A starts at a lower level (≈1.184) before the higher level of transmission is attained (≈1.199), consistent with a sequential

Figure 2. Fabricated plasmonic nanopores and simulated optical response. A) Optical image of a plasmonic nanopore membrane, with 2 large apertures (black squares) for detector alignment. The nanoantennas are discernable as the array of faintly visible dots. Two zooms (TEM images) of inverted-bowtie plasmonic nanopores are shown on the right with varying geometrical features: antenna #1 has a side length of 61 nm, a width of 166 nm, and a gap of 15 nm, and antenna #2 has a side length of 64 nm, a width of 148 nm, and a gap of 25 nm. Scale bars are 50 nm. B) Simulated transmission spectra of the two nanoantennas shown in (A). Antenna #1 has a peak in transmission at a longer wavelength than the excitation laser marked by the black vertical line (i.e., it is red detuned). Antenna #2 has a peak in transmission at a shorter than the excitation laser (i.e., it is blue detuned).
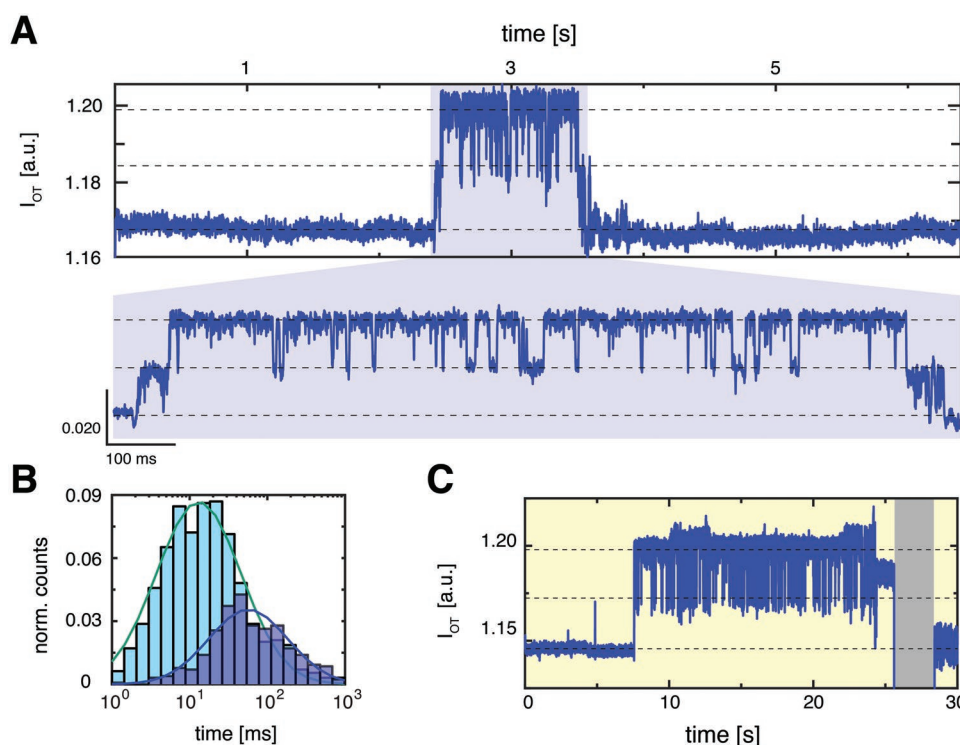
Figure 3. OT signals of 20 nm PS beads trapping in a plasmonic nanopore. A) OT time trace of plasmonic nanopore trapping event at 10 mW of laser power. The start of the event is marked by the sharp increase in OT. The zoom reveals that the signal displays two-level hopping, indicative of two PS beads that are trapped simultaneously, entering and escaping the plasmonic nanopore sequentially over time. B) Histogram of the duration of all events, separated in single- and double-level events (see Experimental Section) 13 ± 2 ms (937 events, fit light-blue line) and 57 ± 9 ms (361, fit dark-blue line). Errors are 95% confidence values on the median. C) OT time trace of a long-duration plasmonic nanopore trapping event at 10 mW of laser power, displaying two-level fluctuations. After switching off the excitation laser, the particles are released. After release, the noise in the baseline was significant, most likely due to a form of contamination entering the aperture.

entering of two particles into the plasmonic nanopore. Correspondingly, the escape of the particles from the trap displays this sequence in reverse. This sequence of stepping events is observed systematically. Additional example traces of PS trapping can be found in Section S4 in the Supporting Information.

The majority of the trapping events are rather short-lived. Figure 3B plots the trapping time histogram of all events, separated into single-level and double-level events (see Experimental Section). The distribution of event durations of both populations follows a log-normal distribution with median trap times of 13 ± 2 ms (light-blue, Figure 3B) and 57 ± 9 ms (dark-blue, Figure 3B) for the single-level and double-level events, respectively. Scatterplots for the different single and double events can be found in Section S5 in the Supporting Information. Around 15% of all events have event durations of over 100 ms, the majority of which displays the dual trap behavior described in the previous paragraph. Figure 3C shows the OT time trace of a very long-lasting dual-trapping event (>1 s; which do happen occasionally, in about 1% of all detected events), which was terminated by turning off the excitation laser. Again, we see similar event characteristics as described above, where two particles enter the trap and produce an ≈4% transmission increase and two-level fluctuations. Upon turning off the incident laser, the OT returns to its baseline value, and the two-level fluctuations have disappeared. More trap-release traces can be found in Section S4 in the Supporting Information.

2.3. Interaction-Assisted Nano-Optical Trapping of Beta-Amylase Proteins

To demonstrate the ability of the nanoantenna to investigate single proteins, we performed nanotweezing experiments using beta-amylase, a globular 200 kDa protein of around 10 nm in size.[35] Before adding protein solution to our flow cell, the OT through the antennas is monitored for 5 min to ensure the absence of spikes in the time trace. **Figure 4** shows two typical OT time traces from two different nanoantennas (the nanoantennas #2 and #1 in Figure 2) after adding beta-amylase at a concentration of 0.03% weight per volume (w/v) to the flow cell. Short transients, discrete signals with a peak amplitude of 0.7% of the OT baseline with a signal-to-noise ratio of 10, can clearly be observed in both traces. These spikes are absent when the antennas are illuminated in transverse polarization (see Section S6 in the Supporting Information) and are only apparent when sufficiently high excitation powers are used (see Section S7 in the Supporting Information). Hence, we attribute these signals to the temporary optical trapping of single protein molecules in the plasmonic nanopore. Event analysis of the dataset in Figure 4 can be found in Section S8 in the Supporting Information and additional traces of beta-amylase trapping experiments can be found in Section S6 in the Supporting Information.

The polarity of the OT signals for protein trapping events depends on the resonant wavelength of the nanoantenna.
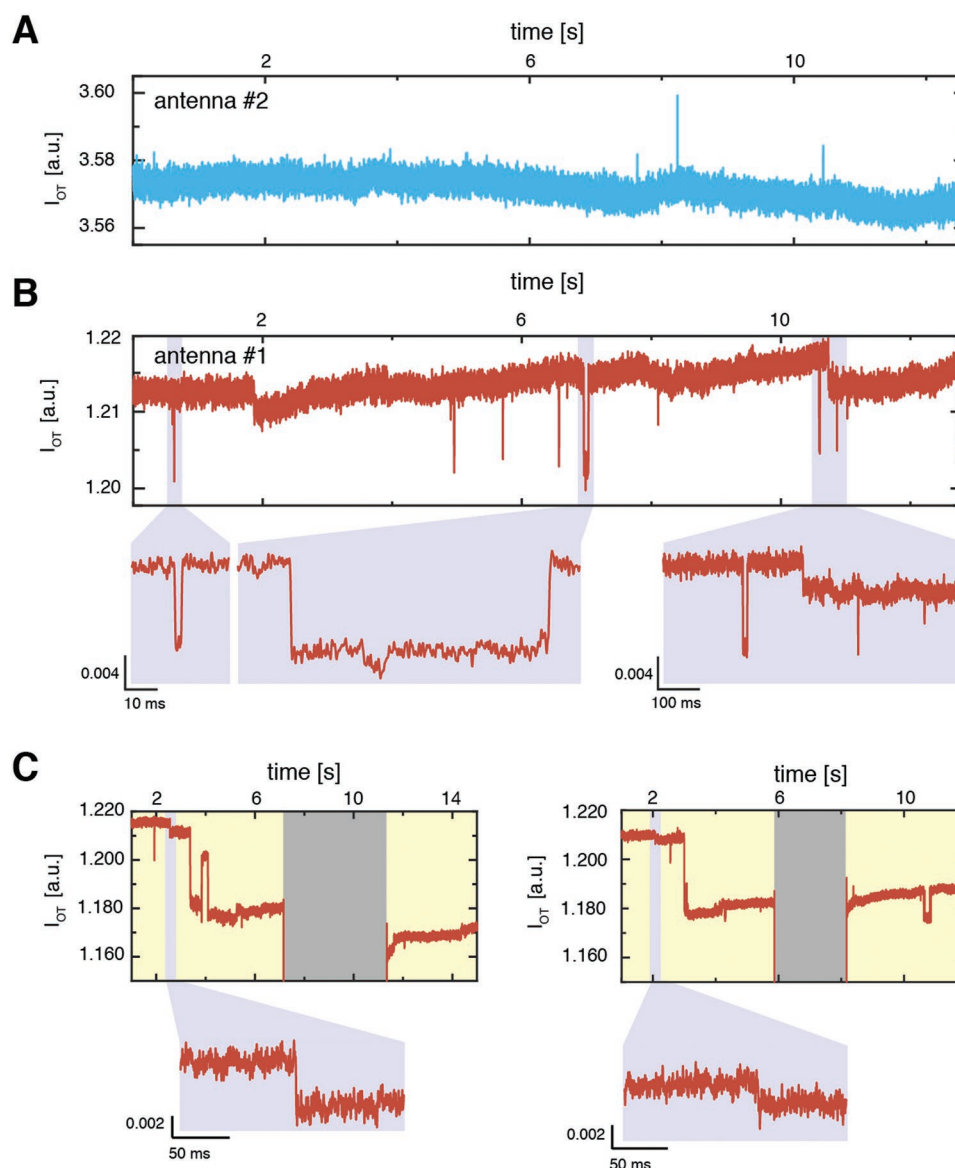
Figure 4. OT signals of beta-amylase protein in plasmonic nanopores. A) OT time trace of beta-amylase protein temporarily trapped in the plasmonic nanopore #2 (Figure 2) at 15 mW of input laser power. Signal are brief *increases* in OT, in accordance with the blue-detuned resonance of this antenna to the excitation laser. B) OT time trace of beta-amylase protein temporarily residing in the plasmonic nanopore #1 (Figure 2) at 15 mW of input laserpower during the same experiment. Signal are *decreases* in OT, in accordance with the red-detuned resonance of this antenna to the excitation laser. Zooms show short-lived (<10 ms) and long-lived (>100 ms) events, with varying amplitudes and event durations. C) Two examples of protein molecules that get denaturing on the surface. The denaturing event is marked by the sudden deep OT decrease which is not released by switching off the excitation laser (black shaded region). The zooms show the protein molecule as it entered the plasmonic nanopore.

Figure 4A shows clear increases in the transmission upon protein entering the aperture. Such increases are indeed expected, since the simulated optical response predicts a blue detuned resonance from the excitation laser (c.f. Figure 2B, right). The presence of a particle in the hotspot will induce a redshift of the resonance of the antenna, resulting in a larger transmission through the aperture. By contrast, Figure 4B shows clear decreases in the transmission, in agreement with simulations for this antenna geometry (c.f. Figure 2B, left). Here, the resonance is red detuned from the excitation laser, resulting in transmission reduction when the protein enters the hotspot. Most of these OT

transients (Figure 4B) are rather short-lived (see Section S8 in the Supporting Information for event statistics), typically lasting less than 10 ms with a few long-lived events lasting over 100 ms—quite similar behavior to the events observed after the addition of PS beads. By reducing the power of the trapping laser, the event durations decrease and the event rate even reduces to near zero for laser powers less than 4 mW (see Section S7 in the Supporting Information). These observations clearly illustrate that optical forces are required to enable observation of the protein.

The event rate varies significantly from antenna to antenna, most likely arising from slight differences in the geometries

**ADVANCED
SCIENCE NEWS**

www.advancedsciencenews.com

**small
methods**

www.small-methods.com

of the antennas. For example, the rates for Figure 4A and 4B are 0.20 ± 0.03 Hz and 0.81 ± 0.03 Hz, respectively. These rates are ballpark similar to the rate of 1.69 Hz measured using nanopore ionic current sensing technique on a 40 nm in diameter nanopore using 1 μM of beta-amylase.[9] Moreover, they are superior to the typical rates quoted for plasmonic nanoaperture tweezers on glass, which are in the range of 10^{-1} to 10^{-4} Hz.[27] These small rates for trapping events can be understood from the sensing region of the plasmonic nanoantenna that is confined to the area in the gap (≈20 nm; see Figure 1C), and hence proteins will most likely also pass through the wings of the antennas where they will not be detected, resulting in missed events. Notably, this is not a problem as, indeed, our plasmonic nanopore devices are not optimized for measuring all events but for trapping of individual proteins.

The longer lasting events do not, contrary to PS bead trapping events, display increased noise fluctuations (c.f. Figure 4B, middle) and the two-step trapping process is not observed, indicating that the trapping of a single protein does not promote the additional trapping of a second protein. The absence of elevated noise levels in our data suggests that Brownian motion is suppressed during the long-lasting events. Spontaneous Brownian fluctuations in the location of the protein in the nanotrap will cause additional fluctuations in the OT[20] which has previously been used to identify the size and conformation of trapped proteins.[25,36] The suppression of Brownian motion could be induced by protein–surface interactions which restrict the translational freedom of the protein in the trap. Indeed, unspecific binding of protein to gold surfaces

is commonly observed[37] and has been used in plasmon resonance sensing to observe protein molecules and study protein–surface binding kinetics.[8] Thus, it appears that both optical forces and surface interactions orchestrate the protein trapping in these structures.

Interestingly, some of the long-lived events display an additional deep OT step that could reveal information about the conformation and state of the trapped protein. Figure 4C shows two examples of such events. Two sequential stages are displayed within the event, an initial step at a shallow level and a second step to a final much deeper OT level (≈3%). After such a sequence of events, the baseline does not recover after switching off the excitation laser (shaded black region). We tentatively interpret these events as protein entering the plasmonic nanoantenna (initial shallow step) and subsequently denaturing on the surface of the antenna (deep final step) to remain there even after the laser is switched off. A denatured protein molecule will produce a larger signal, since it covers a larger part of the most sensitive region in the hotspot and will thus induce a larger resonance shift.[20,38]

2.4. Electrical Regulation of Beta-Amylase Optical Trapping

Plasmonic nanopores have the unique capability that they allow for the application of electrophoretic forces on the biomolecules to influence their behavior inside the plasmonic nanopore as well as to facilitate transport of molecules toward it. **Figure 5**A shows OT time traces of beta-amylase trapping experiments under different transmembrane bias conditions in plasmonic
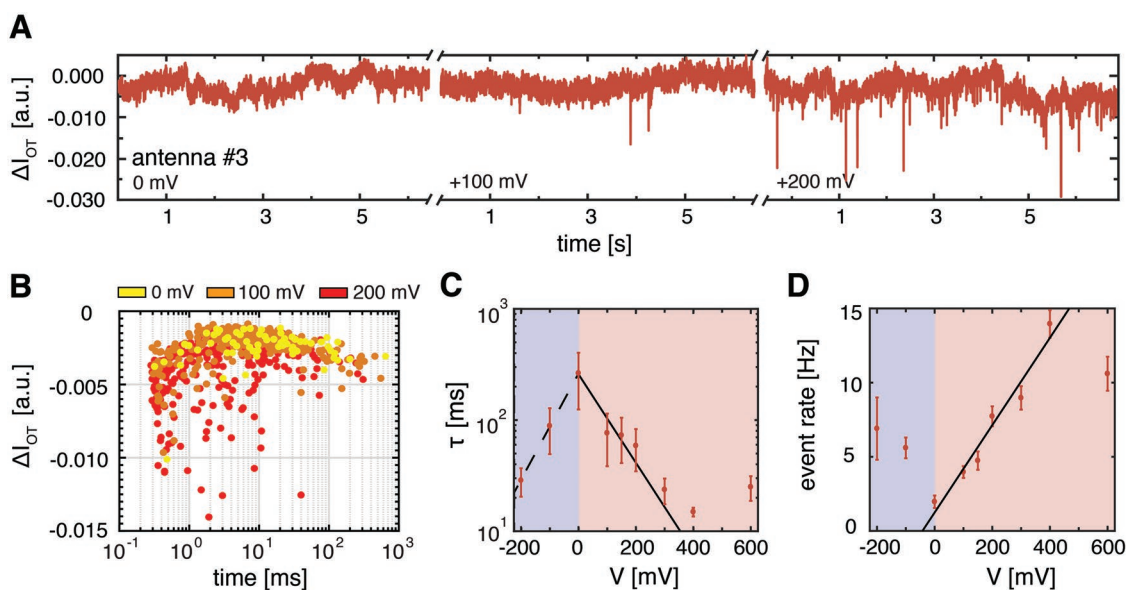

Figure 5. Characterization of the voltage dependence of beta-amylase trapping in a plasmonic nanopore. A) Typical OT time traces of beta-amylase trapping in plasmonic nanopores at 15 mW laser power and under 0, 100, and 200 mV applied bias voltage. B) Scatter diagram of OT event amplitude versus duration for beta-amylase trapping events at 0, 100, and 200 mV bias. C) Characteristic residence time, determined from single-exponential fits to the event duration histogram (see Section S9 in the Supporting Information), versus bias voltage, for negative biasing (blue) and positive biasing (red) of the *trans* chamber. Error bars are standard error of the histogram fits. A clear exponential decreasing trend (solid black line: characteristic voltage $V_0^+ = 92 \pm 29$ mV ($\chi_{red}^2 = 2.1$), dashed line: $V_0^- = 110 \pm 20$ mV [$\chi_{red}^2 < 1.0$]) can be observed. D) Event rate versus bias voltage. A clear linear increase (solid black line, 29 ± 9 Hz V^{-1}, $\chi_{red}^2 = 1.8$) in event rate can be observed for increasing bias voltage. Error bars are standard errors of the histogram fits. All data is recorded on plasmonic nanopore #3, see Section S1 in the Supporting Information.

nanopore #3 (see Section S1 in the Supporting Information and Experimental Section). Again, as expected, downward spikes are clearly discernable, but they become more frequent for larger transmembrane bias. A detailed analysis of the events is shown in Figure 5B, where the average event amplitude is scattered versus duration at 0, 100, and 200 mV. The scatter maps show significant overlap, indicating that the signal amplitude is independent of the bias voltage (see Section S10 in the Supporting Information) and show a broad range of event durations at all voltages probed.

Interestingly, the applied voltage clearly affects the trapping dynamics. Assuming the binding kinetics to dominate the residence times, event duration histograms can be fitted by a single exponential and the characteristic residence time τ can be extracted (see Section S9 in the Supporting Information for histograms and corresponding fits). Figure 5C shows the characteristic residence time τ plotted versus bias voltage. A clear decrease in characteristic residence time can be observed for larger applied transmembrane bias voltages, showing that the transmembrane bias influences the interaction kinetics of the molecules present in the plasmonic nanopore. The characteristic residence time peaks at 0 mV, i.e., in the absence of any transmembrane bias. An exponential fit of $\tau \approx \exp(-V/V_0)$ to the data from 0 to 400 mV (solid black line, Figure 5C, $\chi^2_{red} = 2.1$), reveals a characteristic voltage V_0 of 92 $\pm$ 29 mV. Considering the binding process to be force dependent, this characteristic voltage can reveal information about the spatial extent x_β of the binding-potential well associated with the bound protein state,[39] viz., $x_\beta = kT/F_{E,0}$, where $F_{E,0}$ is the electrical force on the protein molecule at the characteristic voltage. Assuming that the voltage drop is uniform across the 120 nm length of the aperture and using a protein valence of 2e,[9] this translates to a characteristic extent $x_\beta = 16 \pm 4$ nm for the potential well, which is on the order of the size of the protein. If the trapping was purely optical, the trap depth would span the entire thickness of the gold film since the optical field intensity distribution in the antenna is approximately homogenous across the gold film. The smaller observed experimental value is consistent with our finding that the trapping is assisted by protein–surface interactions.

Furthermore, and of great practical interest, a transmembrane bias will enhance the event rate as the electric field emanating from the nanopore will pull molecules toward the sensor.[40,41] Figure 5D shows the event rate as a function of voltage. A clear increase in event rate is observed for larger transmembrane biases, and a clear minimum is present again in the absence of a bias voltage. Surprisingly, an increase in rate is also observed at negative transmembrane biases. This likely arises from proteins that have passed the membrane into the *trans* container (mainly through the large alignment apertures in the membrane during the course of the experiment, see Figure 2A) where they diffuse into the etch pit of the chip. These proteins will be pulled back through the plasmonic pore when a negative bias is applied. The dependence of the event rate on voltage appears to be linear and a fit on the data points from 0 to 400 mV (see Figure 5D, solid black line) shows good agreement with the data $\left(\chi^2_{red} = 1.8\right)$. The linear dependence indicates that the transport toward the pore is diffusion limited,[40] as expected.[9]

3. Conclusion

We have created a plasmonic nanopore sensor for label-free single-molecule manipulation that employs two separate external handles, optical and electrophoretic, for manipulation. Using optical light transmission through plasmonic nano-aperture as readout, we demonstrated optical trapping of single protein molecules, where the residence times in the trap and event rate of the molecules are regulated by the application of an electrical bias voltage.

The observed signal amplitudes from trapped protein in our nanostructures ($\approx$0.7%) are significantly smaller than the protein-induced baseline modulations that were previously reported for double-nanohole antennas on glass[4] (>10%). This can be largely explained by a difference in the excitation modes between those antennas and the ones used in this study; whereas for the double-nanohole antennas a wedge mode[42] is excited, our inverted-bowtie device geometry induced excitation of a plasmonic gap mode. The use of tapered nanostructures might furthermore localize and strengthen the trapping forces. Future optimization of the field confined in the wedge mode may be explored with side tapering of the nanostructures using ion-beam milling strategies that naturally allow for the integration of a nanopore localized to the hotspot.[43]

Interestingly, we do not observe a significantly stronger trapping force in nanoantennas that have a blue detuned resonance with respect to the excitation laser, compared to the red detuned nanoantennas. Plasmonic nano-optical trapping is believed to benefit from self-induced back-action,[22] where the presence of the nanoparticle modifies the optical trap itself. For an antenna with a blue-detuned resonance, the presence of a particle brings the resonance peak closer to the wavelength of excitation. This increases the photon flux through the aperture, which results in an additional force on the object, creating a stiffer trap.[22] On the contrary, a nanoantenna with a red-detuned resonance would constitute a weaker trap.[18] In our protein nanotrapping experiments, we likely do not observe such a difference because the modulation of the transmission is small, diminishing back-action effects.

Finally, the prominent role that the protein–surface interactions play in the optical trapping process of the beta-amylase proteins raises the question if other protein can be optically trapped in these plasmonic nanopores, as now both protein–surface interactions and optical forces must be considered. Optical forces scale with the volume of the trapped object that occupies the hotspot,[44] and hence larger protein complexes should be more efficiently trapped provided they can enter the gap region of the antenna. Moreover, the signal strength scales similarly with the size of the protein, and thus larger protein should also be more easily detected. Nevertheless, trapping experiments with larger proteins (larger than beta-amylase) such as ferritin (450 kDa) and thyroglobuline (600 kDa) did not produce consistent signals. The absence of consistent trapping events for these larger protein suggests that the protein–surface interactions in our case are stronger for beta-amylase than for the other protein tested. Hence, we estimate that the optical forces need to be significantly strengthened for stable protein trapping in the absence of surface interactions.

In summary, we have demonstrated label-free optical detection of single PS beads and single beta-amylase proteins

trapped in a plasmonic nanopore, and we characterized the trapping events under the application of a transmembrane bias. Inverted-bowtie plasmonic nanopores were made by plasma etching and electron-beam lithography on a freestanding SiN membrane and subsequent gold evaporation, resulting in through-hole nanoantennas. We used the intensity of the optical light transmission (OT) through the nanoantenna, modulated by nanoparticle-induced plasmon resonance shifts, as an all-optical readout. First, we verified the optical trapping capabilities of the antenna by trapping 20 nm PS beads that trapped in tandem up to seconds or longer. Next, we demonstrated the ability of the nanoantennas to detect and hold single 200 kDa beta-amylase protein molecules. The absence of enhanced fluctuations in OT during long-lasting trapping events and the failure to release them by switching off the excitation laser, revealed protein–gold surface interactions that aid the optical trapping. Finally, we revealed that the application of a bias voltage could increase the event rate of protein trapping by over an order of magnitude. We furthermore found the residence time to decrease with increasing bias voltage, again indicating surface effects to play a role in the trapping process. Thus, we clearly demonstrated functional applications of an electrophoretic force onto an optically trapped protein, providing the experimenter with orthogonal external control handles at the single-molecule level. This sensor design could, for example, be used to study protein folding–unfolding under a wide variety of different pH conditions and temperature. Future work will focus on improving optical field confinements and optical forces using tapered nanostructures made by ion-beam milling and the demonstration of nanotweezing for a wider variety of different biomolecules.

4. Experimental Section

Sample Fabrication: Plasmonic nanopore devices were fabricated on a 20 nm thin freestanding SiN membrane of around 40×40 μm^2 in size (fabrication details of the membranes are described in ref. [45]). First, a 50 nm thick layer of PMMA 950K resist was spin coated onto the membranes and subsequently an array of inverted bowties was patterned into the resist using electron-beam pattern generator (EBPG5200, Raith) at an exposure dose of 3000 μC cm^{-2}. Then, the pattern was developed in MIBK:IPA 1:3 for 1 min and transferred into the membrane using CHF_3 plasma etching for 100 s, with a flow rate of 50 sccm of CHF_3 and 2.5 sccm of O_2 and at a power of 40 W and a pressure of 8 μbar (Leybold). The residual resist was stripped in an O_2 plasma for 3 min at 100 W (Tepla) and, finally, 5 nm of Ti and 100 nm of Au were evaporated onto the membrane at a rate of 1 and 2 Å s^{-1}, respectively, using an electron-beam evaporator (Temescal).

Experimental Setup: Prior to the experiment, the sample was rinsed in ethanol and ddH_2O and cleaned in O_2 plasma for 30 s (50 W). The sample was mounted in a custom-made PEEK flowcell that allowed for plasmonic nanopore to be optically excited and the transmission light to be collected. The flow cell was filled with either 1× phosphate buffered saline (PBS) or ddH_2O solution, and a voltage was applied over the membrane using a pair of nonpolarizable Ag/AgCl electrodes connected to an amplifier (Model SR570, Stanford Research System). Note that the use of an array of many large inverted-bowtie shaped pores in parallel prevented one from taking single-molecule electrophysiology measurements and the recorded current was only used to verify the correct application of the voltage over the membrane. Subsequently, the laser (M9-A64-0200 laser-diode, Thorlabs, operated in constant-current mode) was focused to a diffraction-limited spot on the sample

using a $60 \times 1.2NA$ water-immersion objective (Olympus) in an inverted microscope setup (see Section S3 in the Supporting Information for a schematic of the optical path). The transmission light was collected using a $10 \times 0.3NA$ objective (Nikon) and projected onto an Avalanche Photo Diode (APD410C/M, Thorlabs). Subsequently, the laser focus was positioned to a 4×4 μm^2 aperture in the gold film and aligned to the detector by maximizing the signal on the APD. The plasmonic nanopore was aligned to the laser focus using a piezoelectric positioning stage (MadCity Labs, Inc) upon maximizing the transmission through the plasmonic nanopore. Prior to the addition of any analyte, the transmission through the plasmonic nanopore was monitored for 5 min to ensure absence of any spikes in the transmission signal. Subsequently, analyte was flushed in and 20 nm PS beads (Thermofischer) were dispensed at a concentration of 0.05% weight per volume (w/v, 1 μM) in ddH_2O with 0.02% w/v SDS (to prevent aggregation of nanoparticles). Beta-amylase proteins (Sigma) were dispensed in 1× PBS at a concentration of 0.03% w/v (15 μM). The voltage dependence was extracted by varying the voltage in an arbitrary sequence to rule out temporal correlations in the observed trends. Data acquisition was performed using custom-made Labview software through a NI DAQ (NI USB-6251, National Instruments) at a sampling rate of 200 kHz.

Event Detection and Analysis: Event detection and analysis were performed using Tranzalyser,[46] a custom-made MATLAB-based software package developed in the lab. All traces were low-pass filtered using a Gaussian filter with a cutoff at 1 kHz for analysis to allow for good signal-to-noise event detection (signal-to-noise ratio of 10). Event detection was done using a 6 sigma threshold spike detection, using a baseline and standard deviation calculated from a moving average window of 10 000 data points.

Single- and double-level events were classified from their maximum peak amplitude in the event. All events with a peak amplitude below the two-level threshold value (0.035, the average value of a double level) were considered single-level events, while those above the threshold level were double-level events (see Section S5 in the Supporting Information). Events durations were calculated from baseline crossing to baseline crossing.

FDTD Simulations: FDTD Solutions (Lumerical Solutions, Inc., Canada) was used to model the optical properties of the inverted-bowtie plasmonic nanoantennas. The inverted bowtie was modeled as a bowtie-shaped aperture in a 100 nm thick gold film with a side length of 60 nm, a width of 140 nm, a 20 nm gap, and 40 nm-in-radius in-plane tip rounding to best resemble the fabricated structures. The antenna was supported by a 20 nm thin silicon-nitride membrane with an RI of 2 that the aperture also perforated. The surrounding medium was modeled as water with an RI of 1.33. Symmetry was used to reduce the computational time. The plasmonic aperture was excited by a pulse from a total-field scattered-field source incident normal to the gold surface, and with the polarization in either the longitudinal or the transverse mode. The light transmission through the nanostructure was calculated by integrating the far-field power flux through a screen placed 350 nm below the membrane and normalized to the total incident power at each frequency.

The optical response of the fabricated nanostructures was simulated by thresholding the planar geometry from a TEM image, using the image import function, and extruding such that the shape penetrated the 100 nm/20 nm gold/SiN stack.

Supporting Information

Supporting Information is available from the Wiley Online Library or from the author.

Acknowledgements

Conflict of Interest

The authors declare no conflict of interest.

Keywords

[1] J. J. Gooding, K. Gaus, *Angew. Chem., Int. Ed.* **2016**, *55*, 11354.
[2] A. Ishijima, T. Yanagida, *Trends Biochem. Sci.* **2001**, *26*, 438.
[3] M. Muthukumar, C. Plesa, C. Dekker, *Phys. Today* **2015**, *68*, 40.
[4] A. A. Al Balushi, A. Kotnala, S. Wheaton, R. M. Gelfand, Y. Rajashekara, R. Gordon, *Analyst* **2015**, *140*, 4760.
[5] S. Howorka, Z. Siwy, *Chem. Soc. Rev.* **2009**, *38*, 2360.
[6] C. Dekker, *Nat. Nanotechnol.* **2007**, *2*, 209.
[7] M. J. Levene, J. Korlach, S. W. Turner, M. Foquet, H. G. Craighead, W. W. Webb, *Science* **2003**, *299*, 682.
[8] A. B. Dahlin, *Analyst* **2015**, *140*, 4748.
[9] C. Plesa, S. W. Kowalczyk, R. Zinsmeester, A. Y. Grosberg, Y. Rabin, C. Dekker, *Nano Lett.* **2013**, *13*, 658.
[10] A. B. Taylor, P. Zijlstra, *ACS Sens.* **2017**, *2*, 1103.
[11] G. Huang, K. Willems, M. Soskine, C. Wloka, G. Maglia, *Nat. Commun.* **2017**, *8*, 935.
[12] J. Larkin, R. Y. Henley, M. Muthukumar, J. K. Rosenstein, M. Wanunu, *Biophys. J.* **2014**, *106*, 696.
[13] H. Bayley, *Clin. Chem.* **2015**, *61*, 25.
[14] A. Squires, E. Atas, A. Meller, *Sci. Rep.* **2015**, *5*, 11643.
[15] O. K. Dudko, J. Mathé, A. Meller, *Methods in Enzymology*, Vol. no. 475, Elsevier, San Diego, CA **2010**, pp. 565–589.
[16] E. C. Yusko, B. R. Bruhn, O. M. Eggenberger, J. Houghtaling, R. C. Rollings, N. C. Walsh, S. Nandivada, M. Pindrus, A. R. Hall, D. Sept, *Nat. Nanotechnol.* **2017**, *12*, 360.
[17] E. C. Yusko, J. M. Johnson, S. Majd, P. Prangkio, R. C. Rollings, J. Li, J. Yang, M. Mayer, *Nat. Nanotechnol.* **2011**, *6*, 253.
[18] P. Mestres, J. Berthelot, S. S. Aćimović, R. Quidant, *Light: Sci. Appl.* **2016**, *5*, e16092.
[19] J.-D. Kim, Y.-G. Lee, *Biomed. Opt. Express* **2014**, *5*, 2471.
[20] Y. Pang, R. Gordon, *Nano Lett.* **2012**, *12*, 402.
[21] C. Chen, M. L. Juan, Y. Li, G. Maes, G. Borghs, P. Van Dorpe, R. Quidant, *Nano Lett.* **2012**, *12*, 125.
[22] M. L. Juan, R. Gordon, Y. Pang, F. Eftekhari, R. Quidant, *Nat. Phys.* **2009**, *5*, 915.
[23] M. L. Juan, M. Righini, R. Quidant, *Nat. Photonics* **2011**, *5*, 349.
[24] S. A. Maier, *Plasmonics: Fundamentals and Applications*, Springer Science & Business Media, New York, USA **2007**.
[25] A. A. Al Balushi, R. Gordon, *ACS Photonics* **2014**, *1*, 389.
[26] A. Kotnala, R. Gordon, *Biomed. Opt. Express* **2014**, *5*, 1886.
[27] R. Gordon, *Opt. Laser Technol.* **2019**, *109*, 328.
[28] I. Ament, J. Prasad, A. Henkel, S. Schmachtel, C. Sönnichsen, *Nano Lett.* **2012**, *12*, 1092.
[29] X. Shi, R. Gao, Y.-L. Ying, W. Si, Y.-F. Chen, Y.-T. Long, *ACS Sens.* **2016**, *1*, 1086.
[30] D. V. Verschueren, S. Pud, X. Shi, L. De Angelis, L. Kuipers, C. Dekker, *ACS Nano* **2018**, https://doi.org/10.1021/acsnano.8b06758.
[31] D. V. Verschueren, W. Yang, C. Dekker, *Nanotechnology* **2018**, *29*, 145302.
[32] H. Guo, T. P. Meyrath, T. Zentgraf, N. Liu, L. Fu, H. Schweizer, H. Giessen, *Opt. Express* **2008**, *16*, 7756.
[33] J. Berthelot, S. Aćimović, M. Juan, M. Kreuzer, J. Renger, R. Quidant, *Nat. Nanotechnol.* **2014**, *9*, 295.
[34] A. Kotnala, R. Gordon, *Nano Lett.* **2014**, *14*, 853.
[35] R. Lundgard, B. Svensson, *Carlsberg Res. Commun.* **1987**, *52*, 313.
[36] S. Wheaton, R. Gordon, *Analyst* **2015**, *140*, 4799.
[37] S. Choi, J. Chae, *J. Micromech. Microeng.* **2010**, *20*, 075015.
[38] P. Zijlstra, P. M. Paulo, M. Orrit, *Nat. Nanotechnol.* **2012**, *7*, 379.
[39] G. I. Bell, *Science* **1978**, *200*, 618.
[40] A. Y. Grosberg, Y. Rabin, *J. Chem. Phys.* **2010**, *133*, 165102.
[41] M. Firnkes, D. Pedone, J. Knezevic, M. Doblinger, U. Rant, *Nano Lett.* **2010**, *10*, 2162.
[42] M. Ghorbanzadeh, S. Jones, M. K. Moravvej-Farshi, R. Gordon, *ACS Photonics* **2017**, *4*, 1108.
[43] M. U. Raza, S. S. S. Peri, L.-C. Ma, S. M. Iqbal, G. Alexandrakis, *Nanotechnology* **2018**, *29*, 435501.
[44] T. Raziman, R. J. Wolke, O. J. Martin, *Faraday Discuss.* **2015**, *178*, 421.
[45] X. J. Janssen, M. P. Jonsson, C. Plesa, G. V. Soni, C. Dekker, N. H. Dekker, *Nanotechnology* **2012**, *23*, 475302.
[46] C. Plesa, C. Dekker, *Nanotechnology* **2015**, *26*, 084003.